Anisotropic magnetic deflagration in single crystals of Gd_{5}Ge_{4}

S. Vélez, J. M. Hernandez, A. García-Santiago, J. Tejada, V. K. Pecharsky, K. A. Gschneidner, Jr., D. L. Schlagel, T. A. Lograsso, and P. V. Santos

Phys. Rev. B **85**, 054432 — Published 28 February 2012

DOI: 10.1103/PhysRevB.85.054432

Anisotropic magnetic deflagration in single crystals of Gd_5Ge_4

S. Vélez,[1,2,*] J. M. Hernandez,[1,2] A. García-Santiago,[1,2] J. Tejada,[1,2] V. K. Pecharsky,[3,4] K. A. Gschneidner, Jr.,[3,4] D. L. Schlagel,[3] T. A. Lograsso,[3] and P. V. Santos[5]

[1] *Grup de Magnetisme, Departament de Física Fonamental, Facultat de Física, Universitat de Barcelona, c. Martí i Franquès 1, planta 4, edifici nou, 08028 Barcelona, Spain*
[2] *Institut de Nanociència i Nanotecnologia IN²UB, Universitat de Barcelona, c. Martí i Franquès 1, planta 3, edifici nou, 08028 Barcelona, Spain*
[3] *The Ames Laboratory, U.S. Department of Energy, Iowa State University, Ames, Iowa 50011-3020, USA*
[4] *Department of Materials Science and Engineering, Iowa State University, Ames, Iowa 50011-2300, USA*
[5] *Paul-Drude-Institut für Festkörperelektronik, Hausvogteiplatz 5-7, 10117 Berlin, Germany*

(Dated: January 11, 2012)

Experimental evidence of the anisotropy of the magnetic deflagration associated with the low-temperature first order antiferromagnetic (AFM) → ferromagnetic (FM) phase-transition in single crystals of Gd_5Ge_4 is reported. The deflagrations were induced by controlled pulses of surface acoustic waves (SAW) allowing to explore both the magnetic field and temperature dependencies on the characteristic times of the phenomenon. The study was done using samples with different geometries and configurations between the SAW pulses and the direction of the applied magnetic field with respect to the three main crystallographic directions of the samples. The effect of temperature is nearly negligible, whereas a strong magnetic field dependence is observed to correlate with the magnetic anisotropy of the sample. Finally, the role of the SAW pulses in both the ignition and formation of the deflagration front was also studied, and we show that the thermal diffusivity of Gd_5Ge_4 must be anisotropic.

PACS numbers: 75.60.Jk, 75.30.Kz, 82.33.Vx

I. INTRODUCTION

The Gd_5Ge_4 intermetallic compound, together with other Si doped $Gd_5(Si_xGe_{1-x})_4$ alloys, has attracted considerable attention over the last few years, principally due to their unusual giant magnetocaloric properties[1–4]. This effect is associated with a first-order AFM↔FM phase transition that occurs simultaneously with a structural transformation[5,6]. The rich phenomenology of these transitions in Gd_5Ge_4 has been broadly studied as a function of temperature, T, and magnetic field, H, using both polycrystalline and single crystalline samples[7–13]. At $T \gtrsim 20$ K, the isothermal magnetic-field-driven AFM↔FM phase transition can be continuously reproduced, but when the sample is cooled at $T \lesssim 10$ K in zero magnetic field, the AFM→FM transition becomes irreversible and exhibits glassy properties[14,15]. This result led the scientific community to believe that the low-temperature magnetocrystallographic ground state of this system was FM O(I),[16] but recent first principles modeling[17–19] of the free energy of the O(I) and O(II) magnetic phases pointed out that the ground state must be AFM O(II).

At low temperatures, the AFM→FM transition in Gd_5Ge_4 can proceed in two different ways. Usually, this transition is rather gradual and takes place over a wide range of magnetic fields, but under certain experimental conditions[20] this phase transformation is abrupt, and this can be identified as a magnetic jump in the magnetic hysteresis cycle, $M(H)$.[6] Historically, such magnetic discontinuities have been called *magnetic avalanches* and they have been also observed in other materials[21–28] which also exhibit a giant magnetocaloric effect[24,29] related to a transition from a kinetically-arrested state to magnetic equilibrium[4,30]. The dynamics of the magnetization of the sample during such transitions have been reported first in molecular magnets[31–39], and later in manganites[40–42] and polycrystalline samples of Gd_5Ge_4[43]. For all these materials it was found that a phase-transition front forms and burns as a consequence of the energy difference between the initial and final states involved, and then it propagates through the sample at a constant speed on the order of a few m/s according to a heat diffusion process (see Appendix A for the basics of the theory of this phenomenon[44] and the definition of the different physical magnitudes involved). The strong similarities between this magnetic phenomenon and a chemical combustion[45] led to call it *magnetic deflagration*.

Magnetic avalanches can appear spontaneously when one of the experimental parameters under control is abruptly changed. However, it does not allow to test the laws of this phenomenon in a controlled way. To solve that, experimentalists have developed technics to trigger the occurrence of magnetic deflagrations under desirable conditions. These consist basically in sending controlled heat pulses to the sample that acts as a spark of flame that ignites the process. Attached resistors[33,35,36,39], electrical contacts made on the sample,[43] or surface acoustic waves (SAW)[32,40] are examples of sources that can be used for this purpose.

However, the test of magnetic deflagration has been limited to only a single law of propagation. In the case of molecular magnets, the speed of the deflagration front is determined by the value of the magnetic field applied along the easy magnetization axis, whereas the transverse field affects the threshold conditions [see for example ref. 38] via their unusual quantum properties[46,47]. In the case of manganites, as well as polycrystalline samples of Gd_5Ge_4, there is no influence, excluding geometrical effects, of the direction of the applied magnetic field on the properties of the deflagration process, whose observed characteristics are the result of averaging the properties along the principal crystallographic axes of the sample due to their random distribution. The goal of this work is to investigate whether the magnetic deflagration in single crystals of Gd_5Ge_4 is anisotropic, and what is the role of each crystallographic axis in both the formation and propagation of the deflagration front.

II. EXPERIMENTAL SET-UP

A large (diameter ca. 4 mm, length ca. 40 mm) single crystal of Gd_5Ge_4 was grown using the tri-arc technique[48]. The Gd metal used to prepare the stoichiometric polycrystalline charge weighing 20 g total was prepared by the Materials Preparation Center of the Ames Laboratory[49], and it was at least 99.99 wt.% pure with respect to all other elements in the periodic table. The Ge was purchased from Meldform Metals, and it was 99.999 wt.% pure. The as-grown single crystal was oriented using backscatter Laue technique. Two different single crystals of Gd_5Ge_4 used in this work were cut from a larger single crystal using spark erosion. Their dimensions referred to the crystallographic directions a, b, and c, were respectively $1.17 \times 2.45 \times 1.04$ mm^3 for sample 1 and $2.40 \times 1.29 \times 1.07$ mm^3 for sample 2.

Fig. 1 shows the schematic of the experimental set-up used in our measurements. The Gd_5Ge_4 samples were mounted using non-magnetic commercial silicon grease on a piezoelectric device [Fig. 1(a)] specially designed to send SAW pulses to the sample. The excitation spectrum of SAW modes with this system is basically determined by the resonances of the interdigital transducer (IDT), whose values are multiple harmonics of a fundamental frequency $f_0 \approx 111$ MHz (see, for example, ref. 32, 40 and 50 for more details). The device is placed inside a commercial Superconducting QUantum Interference Device (SQUID) magnetometer [Fig. 1(b)] able to measure at temperatures down to 1.8 K in magnetic fields up to 5 T. The microwaves for the SAW generation were transported from an external commercial Agilent signal generator to the IDT placed inside the cryostat by means of a coaxial wire that introduces an attenuation smaller than 10 dB.

The SAW pulse induced in the IDT propagates along the lenght of the piezoelectric substrate made of $LiNbO_3$. The crystallinity of the substrate, together with the geometry of the device, provides an amplitude profile of the SAW oscillations in the XZ plane, being therefore the direction of oscillation of the SAW waves out of plane, that is parallel to the y direction [see Fig. 1(a) for the definition of the axes]. Since z is the largest side of the $LiNbO_3$ crystal and x is the perpendicular direction, the amplitude profile of the SAW can be considered practically independent of z, but it depends on x having a maximum at $x = 0$ (that is, the position of the center of the IDT; see for example ref. 51, and references therein, for more details). When desirable experimental conditions (a specific combination of T and H) are reached and stable, a controlled SAW pulse is delivered to ignite the magnetic deflagration process in the Gd_5Ge_4 sample.

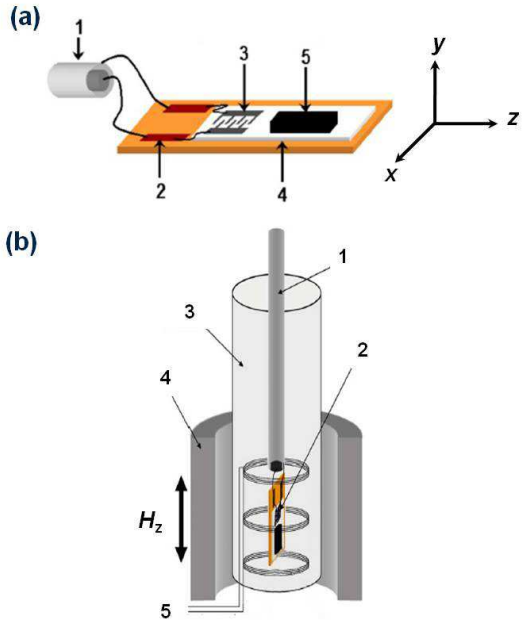

FIG. 1: Experimental set-up. (a) Schematic of the piezoeletric device used. 1, coaxial cable; 2, conducting stripes; 3, IDT; 4, $LiNbO_3$; 5, single crystalline sample of Gd_5Ge_4. (b) View of the spatial distribution of the piezoelectric set-up inside the SQUID magnetometer. 1, coaxial cable; 2, piezoelectric set-up; 3, sample holder; 4, superconducting coils for the magnetic field generation; 5, magnetometer's pick-up coils.

The magnetic field was always applied along the z direction of the sample holder [as shown in Fig. 1(b)], and the piezoelectric set-up was placed inside the pick-up coils of the magnetometer. Two different techniques have been used to obtain magnetic measurements with this system. The first, which is the typical mode, consists in taking dc magnetic measurements by moving the sample through the pick-up coils. It allows one to obtain the absolute magnetic moment of a given sample with a very high precision. This technique has been used to characterize the magnetic properties of the samples, and to verify their magnetic state before and after each induced deflagration. The limitation of this mode is the time it takes to perform each measurement, which is approxi-

mately 30 seconds. The second method consists in measuring directly the voltage from the SQUID-voltmeter, V, without requiring any motion of the sample. Placing the center of the sample in the middle of the inner coils [as shown in Fig. 1(b)], where the sensitivity of the system is maximum, the voltage drop recorded is directly related to the magnetic state of the sample [i.e., $\Delta V \propto \Delta M$]. This technique allows to monitor fast magnetic changes with a time-resolution better than 0.01 ms, so that we can measure the time evolution of the magnetization of the sample during a magnetic deflagration process.

Each single crystal has been studied under different sample/set-up configurations to elucidate the role of each crystallographic axis on the properties of the deflagration phenomenon. Due to geometrical restrictions, four different configurations were available to be explored for each sample. When the magnetic field is applied along the longest side of the crystal, the SAW pulse can be applied to either of the two shorter sides. On the other hand, if the applied field is along one of the shorter directions, the SAW pulse can be applied parallel to the other short side. We will refer to each sample configuration using the following notation: $S_i(x, y, z)$, where i denotes the sample number, and x, y and z, correspond to the orientation of each crystallographic axis of the sample with respect to the coordinate system of the sample holder shown in Fig. 1(a). For example, $S_2(a, b, c)$ refers to sample 2 with its a-axis parallel to the x-direction of the sample holder, b-axis parallel to the y-direction, and c-axis parallel to the z-direction, which is the direction of the magnetic field vector.

III. RESULTS

dc magnetic measurements of the field-driven AFM→FM transition at low temperatures were carried out for each configuration after each sample had been first zero-field-cooled (ZFC) from $T = 50$ K. Fig. 2 shows the AFM→FM transformation and the subsequent removal of the magnetic field in the FM state obtained at 2 K for each independent crystallographic axis using sample 1. The same results were obtained for sample 2, but these are not shown here for brevity. As the magnetic field is increased from zero, the linear slope of the $M(H)$ curves (note that the observed step around $H \sim 8$ kOe when the magnetic field is applied along the c-axis is associated with the spin-flop transition[8]) suggest that the initial state of the sample is purely AFM, and it remains unchanged, until a direction-specific critical magnetic field, H_c, is reached, whose values at 2 K are 28 kOe, 23 kOe and 26 kOe for the a, b and c crystallographic axis, respectively. Above it, the AFM→FM transformation is quite gradual, and it takes place over a field range $\Delta H \sim 4$ kOe. The inset of Fig. 2 shows the fraction $n_{\rm AFM}(H)$ of metastable AFM spins around the transition. At higher temperatures, the critical field $H_c(T)$ decreases with the rate of $\mathrm{d}H_c/\mathrm{d}T \approx -1.5$ kOe/K in the range $2 - 8$ K. All these results are in agreement with previous data reported for single crystalline Gd_5Ge_4 samples[11].

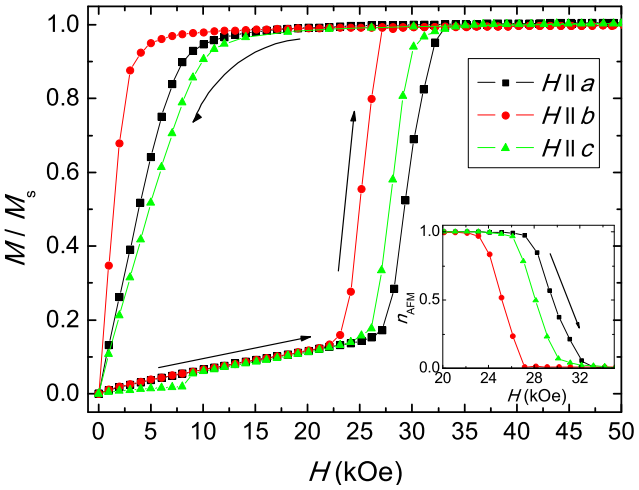

FIG. 2: (color online) Magnetic anisotropy of the field-driven AFM→FM transition and the subsequent removal of the applied magnetic field measured at 2 K after sample 1 had been first ZFC from $T = 50$ K. The inset shows the magnetic-field-dependence of the fraction of metastable AFM spins, $n_{\rm AFM}$, around the magnetocrystallographic transition.

After every crystallographic axis had been magnetically characterized, we proceeded to perform the deflagration experiments on each sample. The two control variables were the initial temperature, T_0, and the applied magnetic field for the ignition, H_{ig}. For each deflagration measurement, the sample was first ZFC from $T = 50$ K to the desired T_0 value. After that, the applied magnetic field was increased slowly to a selected ignition field $H_{ig} \lesssim H_c$, and then a SAW pulse of 100 ms width and 16 dBm was delivered. As a consequence of the pulse, the sample was driven out of the initial equilibrium and for a certain range of experimental T_0 and H_{ig} conditions, a magnetic deflagration was induced. The time evolution of the change in the magnetization of the sample, $\Delta M(t)$, was recorded from the SQUID-voltmeter, where $t = 0$ corresponds to the delivery of the SAW pulse.

Fig. 3(a) shows the resulting $\Delta M(t)$ recorded for the $S_1(c, a, b)$ configuration at $T_0 = 2$ K in the range of ignition fields ($H_{ig} \sim 16.5 - 22.0$ kOe) at which the occurrence of magnetic deflagration was identified and the initial value of $n_{\rm AFM}$ was kept close to one. The data were normalized to the total magnetic drop observed for each case, ΔM_T, which corresponds to the variation of M when the spins of the sample change from the AFM state to the full FM state. This was confirmed from dc magnetic measurements taken before and after each SAW pulse was delivered. For $H_{ig} < 16.5$ kOe, the same kind of measurements revealed that no more than $\sim 10\%$ of the spins of the sample become FM (not shown for simplicity). Moreover, the fraction of transformed spins decreases with decreasing H_{ig}. The abrupt change with

H_{ig} of the number of spins that transforms is a typical feature that shows the self-maintenance of the deflagration process that utilizes the energy of the metastable spins for the occurrence of the full phase transformation when the threshold for the ignition of the deflagration is reached.

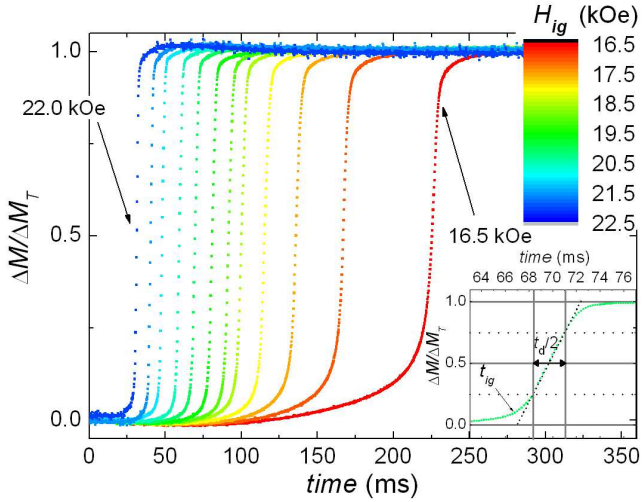

FIG. 3: (color online) Normalized time evolution of the change in the magnetization of the sample, $\Delta M(t)/\Delta M_T$, in the case of $S_1(c,a,b)$ for different ignition fields H_{ig} at $T_0 = 2$ K at which a magnetic deflagration was observed. From right (red) to left (blue), the signals correspond to the data obtained for the values explored from $H_{ig} = 16.5$ kOe to $H_{ig} = 22.0$ kOe in steps of 0.5 kOe. For each measurement, the sample was first ZFC from $T = 50$ K, and then a H_{ig} was applied. After that, a SAW pulse of 100 ms width was delivered at $t = 0$. The inset shows how the t_d and t_{ig} values are obtained from a given signal. The example corresponds to the occurrence of magnetic deflagration at $H_{ig} = 20$ kOe. The diagonal dotted line is a guide to the eye to illustrate the linear evolution of $\Delta M(t)/\Delta M_T$ in the middle part of the avalanche process.

The inset of Fig. 3 shows a zoom of the signal recorded around the occurrence of the deflagration process for $H_{ig} = 20$ kOe. Similar shapes are observed at the other ignition fields. As illustrated, two characteristic times related to the deflagration phenomenon can be identified: t_{ig}, defined as the time that is required to reach the deflagration threshold after the SAW pulse has been switched on; and t_d, defined as the subsequent time interval at which this fast change takes place due to the magnetic deflagration. To determine t_{ig} we have considered the point at which the slope in the $\Delta M(t)$ curve exhibits a sudden change. As it can be seen in Fig. 3, during this time interval, which is much longer than t_d, most of the spins still retain the initial AFM state and only an small change in the magnetization of the sample is observed. To better identify t_d, we have used the middle part of the total magnetic change of the sample, between 0.25 and 0.75 of $\Delta M(t)/\Delta M_T$ (illustrated with horizontal dashed lines), which corresponds to the linear stage of the signal (illustrated with a dotted line). Note that a linear evolution of the magnetization of the sample is indicative of a propagation of a phase front through the sample at constant speed[32,43].

From Fig. 3 it can be easily identified that both characteristic times are strongly influenced by the ignition field, but no remarkable differences were observed when the experimental procedure was repeated at fixed H_{ig} for a wide range of different T_0 values (data not shown). This is an expected behavior that follows from the theoretical expressions given in Appendix A. The speed of the deflagration front, $v(H)$, which is related to $t_d(H)$, only depends on H and is independent on T_0, on condition that the fraction of flammable spins, n_m, is constant [see Eq. (A3)]. This is our case because we restrict our experiments to $n_m = n_{\rm AFM} \simeq 1$. On the other hand, the value of t_{ig} can be theoretically found solving the inequality $\Gamma(H,T) \geq \Gamma_c(H,T)$, where $\Gamma(H,T)$ is the thermal jump over the energy barrier for a single metastable spin, and $\Gamma_c(H,T)$ [see Eq. (A1)] is some critical value of this rate above which the nucleation of the deflagration front should take place[44]. Essentially, this condition is accomplished in our experiments when T is increased enough due to the delivery of a SAW pulse (we will show this effect in section IV.B), providing a certain t_{ig} value. Testing this equation for different T_0 and H_{ig} values, it was confirmed that, whereas a small change in H_{ig} provides a strong change in t_{ig}, the effect of T_0 is practically negligible for a wide range of experimental values. Considering this, we have focused on the field dependencies of the properties of the deflagration phenomenon among the different crystallographic axes and sample configurations.

Fig. 4 shows the dependencies of the characteristic times on the ignition field, $t_d(H_{ig})$ and $t_{ig}(H_{ig})$, obtained for the two samples and for the different configurations explored, split in two groups according to different geometrical arrangements of the crystals in the sample holder: magnetic field applied along the longest side of the crystal [panels (a) and (b)] and magnetic field applied perpendicularly to such side [panels (c) and (d)]. Independently of the specific characteristic times observed for each configuration, several common features are worth noting. When H_{ig} is close to H_c, related to the crystallographic axis of the sample that is parallel to the applied magnetic field, both the ignition and deflagration times are rather fast, taking place only in a few tens of ms and a few ms, respectively. However, as H_{ig} moves down and away from H_c, both times increase progressively showing a non-linear dependence. Moreover, when H_{ig} is reduced far from H_c, the energy supplied by the SAW pulse is no longer sufficient to reach the ignition threshold, and therefore, the deflagration does not take place. Depending on the configuration of the sample, a few deflagrations take place even after the SAW pulse has been switched off [for example, see $S_1(b,a,c)$ in Fig. 4(d) where five deflagrations exhibit $t_{ig} > 100$ ms], indicating again the self-maintaining character of the phenomenon.

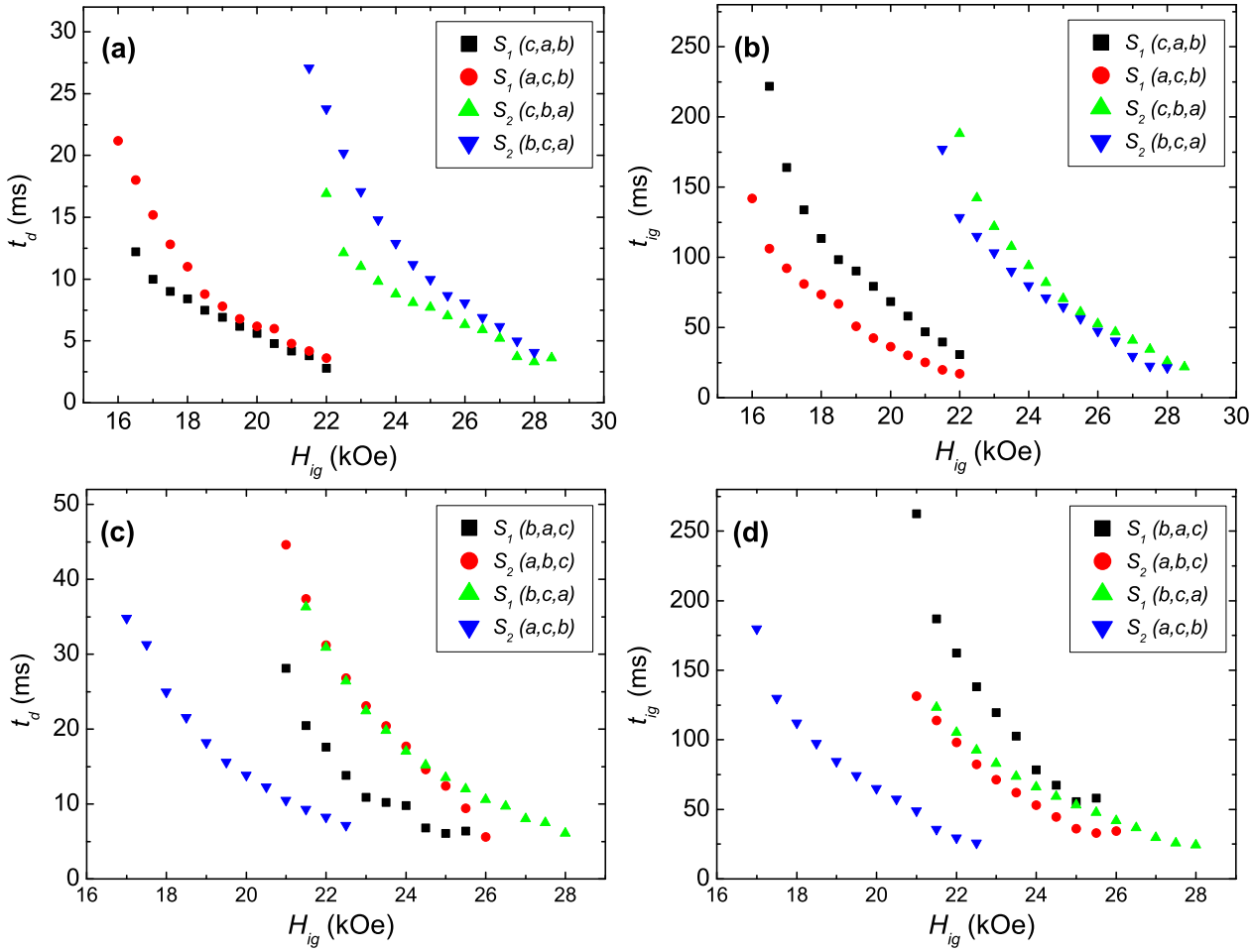

FIG. 4: (color online) The times of deflagration, t_d, and the ignition times, t_{ig}, obtained at different H_{ig} for the two samples studied under different sample/set-up configurations split in two groups. (a) and (b) corresponds to t_d and t_{ig}, respectively, when the applied field is along the longest side of the sample. (c) and (d) corresponds to the same data taken but for the perpendicular configurations.

IV. DISCUSSION

There are two important features to take into account from the time values shown in Fig. 4. On the one hand, for a certain H_{ig} intensity, the observed values of both characteristic times of the magnetic deflagration depend mainly on the crystallographic direction of the sample along which the magnetic field is applied. This follows for instance from strong differences observed between the values obtained for the a and b axes, where the field intervals at which the deflagrations take place do not overlap. However, notice that if the difference $H_{ig} - H_c$, where H_c is the corresponding critical field along which the magnetic field is applied, is taken into account, the characteristic times observed for a given $H_{ig} - H_c$ value become similar for both crystallographic orientations indicating that there is a correlation between the magnetic anisotropy of the sample and the observed deflagration times. On the other hand, the differences between the sets of data $S_1(a, c, b)$ and $S_1(c, a, b)$ [or $S_2(b, c, a)$ and $S_2(c, b, a)$], where the geometrical arrangements of the sample are equivalent (which would imply same lengths of propagation) and the applied magnetic field is along the same crystallographic axis, suggest that additional effects on the properties of the magnetic deflagration may come from the crystallographic orientation of the sample in the XY plane of the sample holder. The aim of this section is to discuss these experimental observations within the framework of the theory of magnetic deflagration to show the connection between magnetic anisotropy and the observed field dependencies, and the role of each crystallographic axis and the SAW pulse on the ignition and propagation of the flame.

A. Comparison of the data with the theory of magnetic deflagration

For simplicity, and because t_d is a more reliable fingerprint of the deflagration phenomenon than t_{ig}, we start

our discussion focusing on this magnitude. This is related to $v(H)$ as $t_d(H) \simeq l_p/v(H)$, where we have defined l_p as the length along which the deflagration front propagates inside the sample. For a planar front propagating along one of the principal crystallographic axis of the sample, the time of propagation of the flame must follow [see Eq. (A3)]

$$t_d^2(H) \approx \frac{\tau_0}{4k_B} \cdot \underbrace{\frac{l_p^2}{\kappa(T_f)}}_{g(l_p,\kappa)} \cdot \underbrace{\frac{U(H)}{T_f(H)} \exp\left[\frac{U(H)}{k_B T_f(H)}\right]}_{f(H)}. \quad (1)$$

Omitting nonessential factors that cannot contribute to any observable difference of the values of $t_d(H)$ between samples and configurations, all the experimental dependencies to be taken into account can be split in two different functions according to their origin. The term $f(H)$ is related to the magnetic field dependencies, i.e., the energy barrier $U(H)$ and the temperature of the flame $T_f(H)$ [see Eq. (A2)], which essentially depends on $\Delta E(H)^{1/4}$ because in all the data reported $n_{\mathrm{AFM}} \simeq 1$. Notice that these field-dependent values correspond to the crystallographic axis along which the magnetic field is applied. On the other hand, geometrical contributions associated with the heat transport have been grouped in $g(l_p, \kappa)$: the propagation length l_p and the thermal diffusivity κ, whose values depend on the crystallographic direction along which the flame propagates. In the case the propagation would not be along one single direction, the $g(l_p, \kappa)$ function should be modified with an appropriate combination of the values of κ and l_p for the axes involved in the process (we will discuss further this question in section IV.B). The characteristic time attempt, τ_0, has been considered as a constant because it is typically a global parameter that characterizes the time-flip of all the spins of a solid and it should be independent of the direction along which the magnetic field is applied.

For any set of data, the main contribution to $t_d(H)$ comes from the $f(H)$ function due to the strong field-dependent term $\exp[U(H)/k_B T_f(H)]$. Notice that this exponential dependence can explain the non-linearity observed in Fig. 4. Since $T_f(H) \propto \Delta E(H)^{1/4}$, the values of $t_d(H)$ should be basically determined by the field dependence of the energy barrier, $U(H)$, whereas $T_f(H)$ may be basically constant for each set of data due to the quite limited range of experimental fields explored. Since the shift in the magnetic field ranges explored between different crystallographic orientations is not too large (it is approximately 20% between the crystallographic axes a and c), we can mostly charge to $U(H)$ the magnetic field dependence of a given sample configuration, whereas the change in $T_f(H)$ may be considered as a minor effect. In this context, the scaling of t_d with $H_{ig} - H_c$ and the magnetic anisotropy of the sample can be directly correlated through the anisotropy of $U(H)$. To better understand it, for a given temperature and crystallographic direction, notice that H_c corresponds to the field at which the effective energy barrier $U(H)$ is reduced enough to get the characteristic time attempt $\tau = \tau_0 \exp[U(H)/k_B T]$ of the order of the time of measurement[47]. According to this, and taking into account that the magnetic field dependence of U should be the same for all crystallographic directions, for the same $H_{ig} - H_c$ values, the strength of the energy barriers would be equal for the three axes, and therefore, similar values of t_d are expected at this same relative field despite the differences that could arise from the geometrical term. Finally, realize that the values obtained for the deflagration time are in agreement with previous values reported in polycrystalline samples[43]. A numerical calculation of t_d and t_{ig} arising from the theory and a comparison with the experimental data is given in Appendix B.

B. Formation of the deflagration front

To be more precise in our further discussion of the geometrical term $g(l_p, \kappa)$, we proceed to compare the data obtained for different configurations when the applied magnetic field is along the same crystallographic direction. In this case, the sets of data are controlled by the same $f(H)$ function. Additionally, for similar geometrical arrangements in the sample holder, l_p should be expected to be not too different. Therefore, the observed differences [for example, see Fig. 4(a)] must be attributed to an anisotropy of κ. However, to better understand this fact, we have to determine, first, what is the role of both the SAW pulse and the sample configuration on the nucleation of the deflagration front and, second, through which length(s)/direction(s) the deflagration front propagates. It could also give a reason for the different observed $t_{ig}(H_{ig})$ values.

Considering both the location and the orientation of the sample over the piezoelectric device, the size of the sample and the quasi-independence of the amplitude of the SAW oscillations in the z direction, the spatial description of any deflagration phenomenon through the sample should be described in two dimensions, in which both the ignition and the propagation of the deflagration can be described in the XY plane. Taking into account the profile of the SAW oscillations in the x direction of the piezoelectric device, it is reasonable to assume that the energy is supplied to the sample mainly at the center of the bottom surface, defined as the (0,0) point in the XY plane. On the other hand, at the range of our working frequencies, the phonon thermalization process should occur in less than 1 ms, whereas the characteristic times involved in our experiments are at least of the order of a few ms. All these features suggest that the interaction of the SAW pulses can be approximated as a spark of fire that essentially heats the sample at the (0,0) point.

The heat supplied to the sample during a SAW pulse diffuses in the XY plane resulting in a thermal rise that depends on the position and the time elapsed from the

ignition of the pulse. Essentially, each isotherm follows an ellipsoidal shape in the XY plane, whose characteristic lengths should follow the relation $l_x/l_y \approx (\kappa_x/\kappa_y)^{1/2}$, where l_i denotes the diffusion length along the i axis of the sample referred to the (0,0) point and κ_i is the thermal diffusivity along this axis. In the case of isotropic diffusion, the characteristic lengths l_x and l_y should be equal. Therefore, in a square geometry, where the two dimensions in the XY plane, L_x and L_y, are equal [this is for instance the case of the data shown in Fig. 4(a) and Fig. 4(b)], the resulting characteristic times of a magnetic deflagration process should be independent on the orientation of these crystallographic axes in the XY plane. However, if one crystallographic orientation would exhibit higher thermal diffusivity, the supplied heat should penetrate easier in such direction breaking the symmetry of the plane and, consequently, the resulting deflagration properties.

To illustrate the effect of the anisotropy of the thermal diffusion, let us take a square geometry in the XY plane and let us consider that a and c are the crystallographic axes involved in this plane for which, for example, $\kappa_a >> \kappa_c$. In such case, and taking into account the geometrical restrictions imposed by the dimensions of the sample and by the point at which the heat is supplied, it can be easily found that the ratio of the ignition time values when κ_a is oriented parallel to the x direction and it is oriented along the y direction, verifies $t_{ig}(\kappa_{a\|}y)/t_{ig}(\kappa_{a\|}x) = t_{ig}(\kappa_{c\|}x)/t_{ig}(\kappa_{c\|}y) \rightarrow 2$. This is because, whereas in the first case the phase front should be generated when $l_x \rightarrow L_x/2$, in the second one it is generated when $l_y \rightarrow L_y$. Therefore, the distance to be covered by the deflagration front formed is different in each case, with the ratio between the deflagration times approaching $t_d(\kappa_{a\|}y)/t_d(\kappa_{a\|}x) = t_d(\kappa_{c\|}x)/t_d(\kappa_{c\|}y) \rightarrow 1/2$.

Focusing on the data shown in Fig. 4(a), when the c crystallographic axis is along the y direction [dots for $S_1(a,c,b)$ and downward triangles for $S_2(b,c,a)$], t_d is higher than when either the b or the a axis is aligned in this direction [squares for $S_1(c,a,b)$ and upward triangles for $S_2(c,b,a)$]. From the phenomenological point of view, the shape of the t_d curves for the two samples are the same when the y direction is parallel to c, and on the other hand, the curves at which c is parallel to x are also similar between them. Moreover, Fig. 4(b) shows that for these sets of data, higher t_{ig} values are obtained when c is parallel to y direction. These findings, together with the expected thermal diffusivity dependencies previously discussed, are indicative of smaller thermal diffusivity along the c axis compared to the b and a axes. From similar arguments, the values obtained in other configurations [for example, the data corresponding to the sets $S_1(b,a,c)$ and $S_2(a,b,c)$ in Fig. 4(c) and 4(d)], suggest that κ_a should be higher than κ_b.

Finally, note that the differences of $t_d(H_{ig})$ values observed between configurations for H applied along the same crystallographic direction cannot be explained by a unique scaling factor for the whole range. It should be attributed to a different ratio of distances covered by the deflagration front depending on the ignition field explored. At magnetic fields close to H_c, the system can be driven out of equilibrium easier. In other words, the deflagration front boundary should form close to the (0,0) point, whereas for smaller fields, its formation is more complicated and it should occur deeper inside the sample where the ignition can take place[43,44]. Therefore, when $H \rightarrow H_c$, the phase front propagates all over the XY surface. However, when H explored is far away from H_c, the anisotropy of κ implies that the deflagration front formed should be different depending on the configuration studied as has been explained before, and then, different propagation lengths are expected. Since the deflagration time is related to the combination of both propagation lengths and thermal diffusivities involved in the process, different ratios of deflagration times are expected for different sample configurations when H_{ig} varies. In conclusion, the difference observed in the magnetic field dependencies should be attributed to the geometric function, $g(l_p,\kappa)$, as a consequence of non-trivial interplay between how the front is generated and how it diffuses in the XY plane.

V. CONCLUSIONS

To summarize, magnetic deflagrations associated with the first order AFM→FM magnetocrystallographic transformations in single crystals of Gd_5Ge_4 have been induced by controlled SAW pulses. The study has been done for different experimental conditions and configurations between the SAW pulses and the applied magnetic field with respect to the crystallographic axes of the samples. As expected, the dynamics of the process fits well within the framework of the magnetic deflagration theory, but the comparison of the data obtained between different configurations have revealed anisotropic character of the process associated with both magnetic and thermal properties of each of the three crystallographic axes of the sample. The main effect comes from the field dependence, which is correlated with the magnetic anisotropy of Gd_5Ge_4 through the anisotropic character of the field dependence of the energy barrier, $U(H)$.

The data obtained suggest that the thermal diffusivity is anisotropic, following $\kappa_a > \kappa_b > \kappa_c$. It plays an important role in the front formation and the subsequent propagation inside the sample due to the fact that the anisotropy of the thermal diffusion can be interpreted as hard and/or easy axes for the occurrence of the phenomenon. Electrical resistivity and magnetoresistance[52], sound propagation and elastic properties[53] have been previously reported to be anisotropic in these and other related alloys, what makes reasonable the conclusion about the anisotropy of the thermal conductivity.

The role of the SAW pulses in the ignition of the magnetic deflagration has been also highlighted. The directionality of the SAW pulse transferred to the sample and the characteristic times in the deflagration process sug-

gest that the pulses act as a unidirectional heater leading to the deflagration process occurring in the perpendicular cross section of the sample. However, we note that for systems in which $t_{ig}(H)$ or $t_d(H)$ are less than, or at least, of the order of 1 ms, the phonon-spin interactions could play an important role in the properties of the magnetic deflagration[54]. Finally, while this work concentrates on the anisotropy of the dynamics of the deflagration phenomena, the authors want to remark that simultaneous to the magnetic deflagration process, a structural change takes place in the system. Further studies should elucidate the very interesting physics of what is happening, principally, inside the magneto-structural burning front.

VI. ACKNOWLEDGEMENTS

S. V. acknowledges financial support from Ministerio de Ciencia e Innovación de España. J. M. H. and A. G.-S. acknowledge support from Universitat de Barcelona. J. T. acknowledges financial support from ICREA Academia. Work at the University of Barcelona was financially supported by the Spanish Government project MAT2008-04535 and Catalan Government project 2009SGR1249. Work at the Ames Laboratory is supported by the U.S. Department of Energy, Office of Basic Energy Science, Division of Materials Science and Engineering under Contract No. DE-AC02-07CH11358 with Iowa State University.

Appendix A: Theory of Magnetic Deflagration

In magnetic deflagration the role of fuel is played by the energy difference between the metastable and the stable states of the system, namely ΔE. This energy difference is related to the intrinsic energy of the metastable ordered magnetic phase plus the Zeeman energy, that comes from the interaction of an external magnetic field H with the spins in the system. On the other hand, the rate of heat transferred from the region of *burning* spins to their *flammable* neighbors is controlled by i) the energy barrier to be overcome by the metastable spins, U; ii) the so-called characteristic time attempt, τ_0; iii) the thermal diffusivity, κ; and iv) the fraction of flammable spins, n_m. The main difference between chemical combustion and magnetic deflagration is that the source of energy for the latter is the reordering of the spins of the system instead of an irreversible chemical reaction. Therefore, magnetic deflagration becomes of special interest due to the non-destructive character of the process.

The theory of magnetic deflagration[44] determines the instability condition that leads a typical broad transition to the occurrence of a deflagration process. When the rate of the thermal jump over the energy barrier for a single metastable spin, Γ, exceeds some critical value, Γ_c, the nucleation of the deflagration front and the subsequent thermal runaway should take place. This critical rate can be written as

$$\Gamma_c = \frac{8k(T)k_BT^2}{U(H)\Delta E(H)n_m l^2}, \tag{A1}$$

where l is some characteristic length, $k(T) = \kappa(T)C(T)$ is the thermal conductivity, and $C(T)$ is the specific heat. The front of propagation is identified as the *flame* of the process, whose characteristic size is $\delta \sim [\kappa(T_f)/\Gamma(T_f)]^{1/2}$, where T_f is the corresponding temperature of the flame, which is given by

$$T_f = \frac{\Theta_D}{\pi}\left[\frac{5n_m\Delta E(H)}{3k_B\Theta_D}\right]^{1/4}, \tag{A2}$$

where Θ_D is the Debye temperature. Finally, in the approximation of a planar burning-front, the speed of the flame is

$$v(H) = \left[\frac{\kappa(T_f)}{\tau_0}\cdot\frac{4k_BT_f(H)}{U(H)}\right]^{1/2}\exp\left[\frac{-U(H)}{2k_BT_f(H)}\right]. \tag{A3}$$

Appendix B: Matching between theoretical and experimental values

From previously reported data[43] of the magnetic deflagration in a polycrystalline sample of Gd_5Ge_4, T_f was estimated to be around 30 K. Taking into account the discussion given above about the $T_f(H)$ values of the different crystallographic axis, and that the magnetic properties of a polycrystal are averaged, we can assume that $T_f \sim 30$ K is a good estimate of the temperature of the flame in all observed deflagrations. Thus, the thermal diffusivity of the sample is estimated to be[55] $\kappa(T_f) \sim 3\cdot 10^{-5}$ m^2/s. Taking $l_p \sim 1$ mm, $\tau_0 \sim 10^{-7}$ s, and considering that in our experimental field range $U(H)$ should be around $200-300$ K, one gets from Eq. (1), $t_d \sim 10$ ms, which is in good agreement with our observations. The other interesting parameter to test is the width of the flame δ, which can be found through $\delta \sim [\kappa(T_f)/\Gamma(T_f)]^{1/2}$. Here, $\Gamma(T_f) = \tau_0^{-1}\exp[-U/k_BT_f]$, so an upper limit can be estimated to be $\delta_{\max} \sim 0.1$ mm, which means that a flame of this size can form and propagate inside the sample.

The values of the ignition time can be estimated solving the inequality $\Gamma \gtrsim \Gamma_c$. Using[55] $k(T) \sim 8$ J/s·K and all the values estimated above for the magnitudes appearing in Eq. (A1), the condition $\Gamma \sim \Gamma_c$ should be accomplished for $T_{ig} \sim 12$ K. In other words, the deflagration process may take place if the temperature in some part of the sample is quickly raised above T_{ig}[44]. Although in our experiments this cannot be done fast enough, we may assume that this condition could be accomplished if a certain volume of spins of the sample, of the order of the spins contained in the burning front, are heated around this temperature. Since the upper limit

for the width of the deflagration front is $\delta_{\max} \sim 0.1$ mm, the upper limit for this volume is on the order of 10% of the total volume of the sample. Then, we proceed to estimate the thermal rise experimented by this volume due to a SAW pulse of $\Delta t = 100$ ms. Assuming a good transfer between the pulse and the sample, the transferred energy is estimated to be $E_{\rm SAW} = P \cdot \delta t \sim 10$ mW $\cdot$ 0.1 s = 1 mJ. On the other hand, the heating of N_δ mols can be expressed as $dT = dE_{\rm SAW}/C(T)N_\delta$. In the region of interest, $C(T) = \alpha T^3$, where α is a well-known constant whose value is[6] 0.7 J/mol·K^4. Therefore, the final temperature of this volume is given by $T_\delta^4 = 4\Delta E_{\rm SAW}/\alpha N_\delta + T_0^4$, where T_0 is the initial temperature. In our case, the mass to be heated is $m_\delta \sim 1$ mg, so that $N_\delta \sim 10^{-6}$ mol. Replacing all the magnitudes in this equation by numerical values, one gets $T_\delta \sim 9$ K, which is in agreement with the expected ignition temperature, $T_{ig} \sim 12$ K.

* Electronic address: svelez@ubxlab.com

[1] V. K. Pecharsky and K. A. Gschneidner, Jr., Phys. Rev. Lett. **78**, 4494 (1997).

[2] W. Choe, V. K. Pecharsky, A. O. Pecharsky, K. A. Gschneidner, Jr., V. G. Young, and G. J. Miller, Phys. Rev. Lett. **84**, 4617 (2000).

[3] V. K. Pecharsky, A. P. Holm, K. A. Gschneidner, Jr., and R. Rink, Phys. Rev. Lett. **91**, 197204 (2003).

[4] L. S. Sharath Chandra, S. Pandya, P. N. Vishwakarma, D. Jain, and V. Ganesan, Phys. Rev. B **79**, 052402 (2009).

[5] L. Morellon, J. Blasco, P. A. Algarabel, and M. R. Ibarra, Phys. Rev. B **62**, 1022 (2000).

[6] E. M. Levin, V. K. Pecharsky, K. A. Gschneidner, Jr., and G. J. Miller, Phys. Rev. B **64**, 235103 (2001).

[7] E. M. Levin, K. A. Gschneidner, Jr., and V. K. Pecharsky, Phys. Rev. B **65**, 214427 (2002).

[8] E. M. Levin, K. A. Gschneidner, Jr., T. A. Lograsso, D. L. Schlagel, and V. K. Pecharsky, Phys. Rev. B **69**, 144428 (2004).

[9] M. K. Chattopadhyay, M. A. Manekar, A. O. Pecharsky, V. K. Pecharsky, K. A. Gschneidner, Jr., J. Moore, G. K. Perkins, Y. V. Bugoslavsky, S. B. Roy, P. Chaddah, et al., Phys. Rev. B **70**, 214421 (2004).

[10] H. Tang, V. K. Pecharsky, K. A. Gschneidner, Jr., and A. O. Pecharsky, Phys. Rev. B **69**, 064410 (2004).

[11] Z. W. Ouyang, V. K. Pecharsky, K. A. Gschneidner, Jr., D. L. Schlagel, and T. A. Lograsso, Phys. Rev. B **74**, 024401 (2006).

[12] F. Casanova, A. Labarta, X. Batlle, J. Marcos, L. Mañosa, A. Planes, and S. de Brion, Phys. Rev. B **69**, 104416 (2004).

[13] Z. W. Ouyang, Z. C. Xia, Y. C. Wang, and G. H. Rao, J. Appl. Phys. **109**, 023901 (2011).

[14] S. B. Roy, M. K. Chattopadhyay, P. Chaddah, J. D. Moore, G. K. Perkins, L. F. Cohen, K. A. Gschneidner, Jr., and V. K. Pecharsky, Phys. Rev. B **74**, 012403 (2006).

[15] S. B. Roy, M. K. Chattopadhyay, A. Banerjee, P. Chaddah, J. D. Moore, G. K. Perkins, L. F. Cohen, K. A. Gschneidner, Jr., and V. K. Pecharsky, Phys. Rev. B **75**, 184410 (2007).

[16] O(I) [O(II)] is a common notation of the low-volume [high-volume] orthorhombic polymorph of Gd_5Ge_4. See V. K. Pecharsky and K. A. Gschneidner, Jr., Pure Appl. Chem. **79**, 1383 (2007) for details.

[17] D. Paudyal, V. K. Pecharsky, K. A. Gschneidner, Jr., and B. N. Harmon, Phys. Rev. B **75**, 094427 (2007).

[18] D. Paudyal, V. K. Pecharsky, and K. A. Gschneidner, Jr., J. Phys.: Condens. Matter **20**, 235235 (2008).

[19] D. Paudyal, Y. Mudryk, V. K. Pecharsky, and K. A. Gschneidner, Jr., Phys. Rev. B **82**, 144413 (2010).

[20] Basically, the experimental conditions that help the occurence of avalanches are: i) that the initial magnetic phase of the sample is mostly AFM; ii) very low temperatures; iii) big samples; and iv) fast sweeping rates of the applied magnetic field.

[21] C. Paulsen, J. G. Park, B. Barbara, R. Sessoli, and A. Caneschi, J. Magn. Magn. Mater. **140-144**, 1891 (1995).

[22] E. del Barco, J. M. Hernandez, M. Sales, J. Tejada, H. Rakoto, J. M. Broto, and E. M. Chudnovsky, Phys. Rev. B **60**, 11898 (1999).

[23] R. Mahendiran, A. Maignan, S. Hébert, C. Martin, M. Hervieu, B. Raveau, J. F. Mitchell, and P. Schiffer, Phys. Rev. Lett. **89**, 286602 (2002).

[24] L. Ghivelder, R. S. Freitas, M. G. das Virgens, M. A. Continentino, H. Martinho, L. Granja, M. Quintero, G. Leyva, P. Levy, and F. Parisi, Phys. Rev. B **69**, 214414 (2004).

[25] L. M. Fisher, A. V. Kalinov, I. F. Voloshin, N. A. Babushkina, D. I. Khomskii, Y. Zhang, and T. T. M. Palstra, Phys. Rev. B **70**, 212411 (2004).

[26] D. S. Rana and S. K. Malik, Phys. Rev. B **74**, 052407 (2006).

[27] V. Hardy, S. Majumdar, S. J. Crowe, M. R. Lees, D. M. Paul, L. Hervé, A. Maignan, S. Hébert, C. Martin, C. Yaicle, et al., Phys. Rev. B **69**, 020407 (2004).

[28] B. Maji, K. G. Suresh, and A. K. Nigam, Europhys. Lett. **91**, 37007 (2010).

[29] F. Fominaya, J. Villain, P. Gandit, J. Chaussy, and A. Caneschi, Phys. Rev. Lett. **79**, 1126 (1997).

[30] L. Ghivelder and F. Parisi, Phys. Rev. B **71**, 184425 (2005).

[31] Y. Suzuki, M. P. Sarachik, E. M. Chudnovsky, S. McHugh, R. Gonzalez-Rubio, N. Avraham, Y. Myasoedov, E. Zeldov, H. Shtrikman, N. E. Chakov, and G. Christou, Phys. Rev. Lett. **95**, 147201 (2005).

[32] A. Hernández-Mínguez, J. M. Hernandez, F. Macià, A. García-Santiago, J. Tejada, and P. V. Santos, Phys. Rev. Lett. **95**, 217205 (2005).

[33] S. McHugh, R. Jaafar, M. P. Sarachik, Y. Myasoedov, A. Finkler, H. Shtrikman, E. Zeldov, R. Bagai, and G. Christou, Phys. Rev. B **76**, 172410 (2007).

[34] A. Hernandez-Minguez, C. Carbonell-Cortes, R. Amigo, J. M. Hernandez, J. Tejada, and E. M. Chudnovsky, Appl. Phys. Lett. **91**, 202502 (2007).

[35] S. McHugh, R. Jaafar, M. P. Sarachik, Y. Myasoedov, A. Finkler, E. Zeldov, R. Bagai, and G. Christou, Phys. Rev. B **80**, 024403 (2009).

[36] S. McHugh, B. Wen, X. Ma, M. P. Sarachik, Y. Myasoedov, E. Zeldov, R. Bagai, and G. Christou, Phys. Rev. B **79**, 174413 (2009).

[37] W. Decelle, J. Vanacken, V. V. Moshchalkov, J. Tejada,

J. M. Hernández, and F. Macià, Phys. Rev. Lett. **102**, 027203 (2009).
[38] F. Macià, J. M. Hernandez, J. Tejada, S. Datta, S. Hill, C. Lampropoulos, and G. Christou, Phys. Rev. B **79**, 092403 (2009).
[39] D. Villuendas, D. Gheorghe, A. Hernández-Mínguez, F. Macià, J. M. Hernandez, J. Tejada, and R. J. Wijngaarden, Europhys. Lett. **84**, 67010 (2008).
[40] F. Macià, A. Hernández-Mínguez, G. Abril, J. M. Hernandez, A. García-Santiago, J. Tejada, F. Parisi, and P. V. Santos, Phys. Rev. B **76**, 174424 (2007).
[41] F. Macià, G. Abril, A. Hernández-Mínguez, J. M. Hernandez, J. Tejada, and F. Parisi, Phys. Rev. B **77**, 012403 (2008).
[42] F. Macià, G. Abril, J. M. Hernandez, and J. Tejada, J. Phys.: Cond. Matter **21**, 406005 (2009).
[43] S. Velez, J. M. Hernandez, A. Fernandez, F. Macià, C. Magen, P. A. Algarabel, J. Tejada, and E. M. Chudnovsky, Phys. Rev. B **81**, 064437 (2010).
[44] D. A. Garanin and E. M. Chudnovsky, Phys. Rev. B **76**, 054410 (2007).
[45] I. Glassman, *Combustion* (Academic, New York, 1996).
[46] J. R. Friedman, M. P. Sarachik, J. Tejada, and R. Ziolo, Phys. Rev. Lett. **76**, 3830 (1996).
[47] E. M. Chudnovsky and J. Tejada, *Macroscopic Quantum Tunneling of the Magnetic Moment* (Cambridge University Press, Cambridge, England, 1998).
[48] D. L. Schlagel, T. A. Lograsso, A. O. Pecharsky, and J. A. Sempaio, in: Light Metals, H. Kvande, Ed. (TMS, Minerals, Metals, and Materials Society, Warrenton, PA) p. 1177 (2005).
[49] Materials Preparation Center, Ames Laboratory of US DOE, Ames, Iowa, USA, www.ameslab.gov/mpc.
[50] K. Yamanouchi, C. H. S. Lee, K. Yamamoto, T. Meguro, and H. Odagawa, *Proceedings of the 1992 IEEE Ultrasonic Symposium* (IEEE, New York, 1992).
[51] M. M. de Lima Jr and P. V. Santos, Rep. Prog. Phys. **68**, 1639 (2005).
[52] H. Tang, V. K. Pecharsky, G. D. Samolyuk, M. Zou, K. A. Gschneidner, Jr., V. P. Antropov, D. L. Schlagel, and T. A. Lograsso, Phys. Rev. Lett. **93**, 237203 (2004).
[53] O. Svitelskiy, A. Suslov, D. L. Schlagel, T. A. Lograsso, K. A. Gschneidner, Jr., and V. K. Pecharsky, Phys. Rev. B **74**, 184105 (2006).
[54] A. Hernández-Mínguez, F. Macià, J. M. Hernandez, J. Tejada, and P. V. Santos, J. Magn. Magn. Mater. **320**, 1457 (2008).
[55] S. Fujieda, Y. Hasegawa, A. Fujita, and K. Fukamichi, J. Appl. Phys. **95**, 2429 (2004).